Available online at www.sciencedirect.com
SCIENCE DIRECT®
International Journal of Heat and Fluid Flow 24 (2003) 345–355
International Journal of HEAT AND FLUID FLOW
www.elsevier.com/locate/ijhff

Recent developments in the measurement of convective heat transfer rates by laser interferometry

D. Naylor *

Department of Mechanical, Aerospace and Industrial Engineering, Ryerson University, 350 Victoria Street, Toronto, Ont., Canada M5B 2K3

Abstract

In this paper, a brief introduction is given to the principle of operation of both classical and holographic interferometers, which are commonly used for the measurement of convective heat transfer rates. Some of the optical considerations, as well as the limitations of this experimental technique are highlighted. With this background, some recent developments in laser interferometry are discussed for both two- and three-dimensional temperature fields, with an emphasis on techniques for measuring local convective heat flux rates.
© 2003 Elsevier Science Inc. All rights reserved.

Keywords: Interferometry; Convection; Tomography; Holography

1. Introduction

Many optical techniques have been developed that utilize the variation of refractive index to measure the temperature field in a fluid. In several relatively recent publications, methods such as laser speckle photography (Guo et al., 1995; Asseban et al., 2000), laser deflection techniques (El Ammouri and Taine, 1994; Zhang et al., 1989), Talbot interferometry (Shakher and Nirala, 1999) and quantitative Schlieren (Tanda, 1993) have been successfully applied. These methods are based primarily upon on the deflection of light rays produced by refraction effects. In other optical techniques the temperature field is inferred by measuring the phase differences of light rays caused by variations in refractive index. In these methods, beam refraction produced by the phase object being studied is undesirable and represents a source of measurement error. With reference to recent publications, such methods include classical interferometry (Mishra et al., 1999; Duarte et al., 2001), shearing interferometry (Wozniak and Siekmann, 1995; Ramesh and Merzkirch, 2001) and holographic interferometry (Iida et al., 1996; Inada et al., 1999; Nakano et al., 2001; Herman and Kang, 2001; Liou, 2001).

The current review focuses on the use of classical and holographic interferometry for the measurement of convective heat transfer. Interferometry has been widely used for full-field temperature measurement and for the evaluation of local heat transfer rates, with some of the earliest convection measurements dating back to the 1930s and 1940s (Kennard, 1939; Eckert and Soehngen, 1948). Until recently, most studies were performed by classical two-beam interferometry, using a Mach–Zehnder interferometer (MZI) or similar instrument. But, in the past ten years, the use of holographic interferometry has become increasingly widespread for measurements in convection.

Publications in the heat transfer literature over the past few years indicate that both classical and holographic interferometers are widely used. In the recent literature, Kwak and Song (2000) applied a MZI to measure free convection from downward-facing finned plate and Yoon et al. (2001) used a holographic interferometer to study freezing of water near a horizontal cylinder. For a variety of problems, interferometry can provide non-intrusive temperature field visualization and local heat transfer data that are well-suited for the verification of numerical predictions. In fact, there appears to have been a significant resurgence of interest in interferometry that has paralleled the rapid developments in heat transfer modeling.

* Tel.: +1-416-979-5303; fax: +1-416-979-5265.
E-mail address: dnaylor@ryerson.ca (D. Naylor).

0142-727X/03/$ - see front matter © 2003 Elsevier Science Inc. All rights reserved.
doi:10.1016/S0142-727X(03)00021-3

Nomenclature

C	constant in Eq. (1)
c_i	coefficient in Eqs. (3) and (4)
d	wedge fringe spacing (m)
G	Gladstone-Dale constant (m^3/kg)
Gr	Grashof number
h	convective heat transfer coefficient ($W/m^2\,K$)
k	thermal conductivity (W/m K)
L	length of the model in the beam direction (m)
m	exponent of the power function temperature variation
n	refractive index
Nu	local Nusselt number
P	absolute gas pressure (Pa)
p	distance, defined in Fig. 6 (m)
Pr	Prandtl number
R	ideal gas constant (J/kg K)
Ra	Rayleigh number
r	radial coordinate (m)
T	temperature (K)
$\overline{T}$	actual beam-average fluid temperature (K)
T_f	measured average fluid temperature (K)
T_h	local fluid temperature at the exit of the test section (K)
x, y	Cartesian coordinates (m)

Greeks

α	wedge fringe angle (rad)
δ	Dirac delta function
ε	fringe shift order
ϕ	angle, defined in Fig. 6 (rad)
λ_o	laser vacuum wavelength (m)
θ	projection angle (rad)

Subscripts

ref	associated with the reference beam
s	evaluated at the surface temperature
∞	evaluated at the surface temperature

In this paper, a brief description is given of the principle of operation of classical and holographic interferometers. With this background, recent developments in laser interferometry are discussed for both two and three-dimensional temperature fields, with an emphasis on techniques for evaluating local heat flux rates. For two-dimensional temperature fields, a method recently developed for measuring low heat flux rates is discussed. For three-dimensional problems, results obtained by interferometric tomography are briefly reviewed. For three-dimensional geometries that are not amenable to tomography, a discussion of "beam-averaged" heat flux measurements is presented. Several applications are used to illustrate these optical methods.

2. Classical interferometry

One of the most common instruments used for classical two-beam interferometry is the MZI. Fig. 1 shows a sketch of the optical setup of a MZI. The input optics consist of a beam expander and parabolic mirror, which are used to expand the laser into a large diameter collimated beam. At the first beam splitter, the expanded beam is divided into two beams, which are initially in phase. As shown in Fig. 1, the test beam travels past the experimental model and the reference beam travels through the ambient air, which has uniform temperature. Because of the change in refractive index with temperature of the fluid in the experimental model, the speed of light near the model surface is different than in the reference beam. As a result, the test beam undergoes a phase shift relative to the reference beam. When the two beams are recombined at the second beam splitter, this phase shift produces interference fringes in the output beam, which can be observed and recorded in real-time.

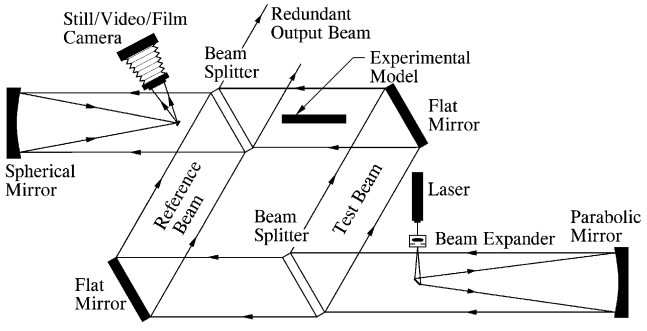

Fig. 1. Sketch of optical setup of a MZI.

For classical interferometry, very high precision optical components must be used to obtain an interference fringe field with low distortion. From the point where the laser beam is split, to the point where the beams are recombined, all wave front distortions caused by the optical components must be kept to a minimum. Typically, this requires that the beam splitters, flat mirrors and test section optical windows (if required) be flat to approximately one twentieth of a wavelength of light ($\lambda/20$). Also, parallelism of the two beam splitter surfaces must be maintained to better than 5 arc seconds. If a large diameter test beam is required, the optical components can be expensive. For example, a single 20 cm diameter beam splitter currently costs about 4000 US dollars. In addition, if the test section is to be pressur-

ized, thick optical windows must be used to reduce the stress-induced deflection of the window surfaces. Further details of the design and operation of MZIs are given by Goldstein (1970) and Hauf and Grigull (1970).

It is important to note that many optical configurations other than the MZI have been used for classical interferometry. One noteworthy configuration is the Twyman–Green interferometer. In this optical setup, the test beam makes a double pass through the experimental model. This results in double the sensitivity, compared to a MZI. This configuration can be useful for increasing the total fringe order when measurements must be made at a low temperature difference or with a test model that is short in the light beam direction. Papple and Tarasuk (1985) have used a Twyman–Green interferometer to study free convection around a vertical cylinder in air. Also, Fröhlich et al. (1996) have studied the adiabatic heating of SF_6 caused by the so-called "piston effect" using this optical setup. Other optical configurations that use a multiple-pass of the test beam have also been proposed (Sheng-jie, 1983; Yan and Cha, 1998).

3. Holographic interferometry

The detailed theory of holography is too involved to discuss fully here. Only a brief description will be given. The reader is referred to the literature (Vest, 1979; Mayinger, 1994; Kreis, 1996) for more detailed coverage.

Fig. 2 shows a typical optical setup of a holographic interferometer for convective heat transfer measurements. It can be seen that the optical configuration has many similarities to that of a MZI. Comparing Figs. 1 and 2 reveals that one main difference between a MZI and a holographic interferometer is that the last beam splitter is replaced with a holographic plate. As in classical interferometry, a beam splitter initially divides the laser light into two beams. One beam, called the reference beam, by-passes the model and strikes the holographic plate. The other beam, called the object beam, passes through the test section prior to reaching the plate. Note that when holography is applied to the measurement of refractive index, the test fluid under study is called a phase object. This is because the test fluid mainly affects the phase distribution of the light beam.

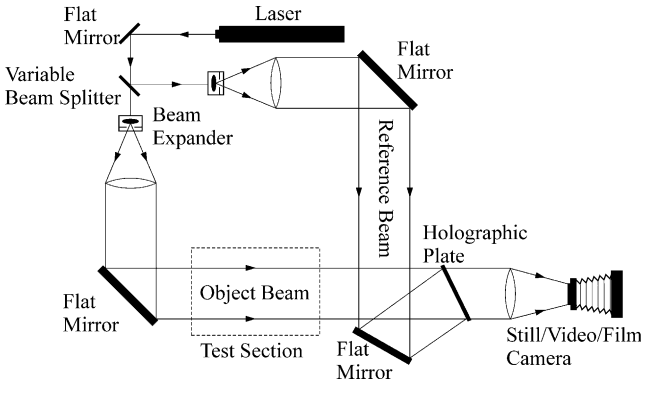

Fig. 2. Sketch of optical setup of a holographic interferometer.

As discussed in the previous section, with a MZI the interferogram is formed by the interference of the test beam with the reference beam, while the heat transfer process of interest is occurring in the test beam. In contrast, for holographic interferometry, the interferogram is generated by the interference of two object beams, which occur at different times. Two object waves, one with and one without heat transfer, are superposed to produce the interferogram. Two methods are commonly used to achieve this superposition: (i) double exposure holographic interferometry and (ii) real time holographic interferometry.

In the double exposure method, two different object beams are recorded on the same holographic plate using multiple exposures. First the holographic plate is exposed to the object beam with the experimental model at thermal equilibrium with the surroundings. Then, the model is heated (or cooled) to the desired test condition and the holographic plate is exposed for the second time. The holographic plate is then developed and repositioned in the interferometer. When this multiple exposure hologram is illuminated by the reference wave, the hologram behaves like a complex refraction grating, causing both object waves to be reconstructed simultaneously. These two waves combine to produce an interferogram.

The double exposure method has been used frequently for convective heat transfer studies (e.g. Cha and Cha, 1996). However, the main drawback of this method is that it produces a static interferogram, which is a "snap-shot" of phase object. This limitation is overcome in the real time method, which is described next.

As the name implies, the real time method permits continuous observation of the temperature field. The first step is that the holographic plate is exposed to the unheated model i.e., the comparison wave and reference wave. The plate, with this single exposure, is then developed. The next step is that the experimental model is heated to the desired conditions. The hologram is repositioned in the interferometer and is illuminated with the new object wave (measurement wave) and the reference wave. The measurement wave passes through the hologram and interferes with the comparison wave of the unheated model, which is reconstructed by the reference wave. The resulting output is a continuous interference pattern, which can be observed in real time.

It should be noted from the above discussion that the optical components of a holographic interferometer do

not require the same precision as those of a MZI. Because both the comparison and measurement waves are affected in precisely the same way by any optical imperfections, the phase difference between the two beams is caused only by refractive index variations in the phase object. So, for example, standard commercial glass can be used instead of precision optical windows to seal off the ends of a test model. In fact, the ability to use less expensive optical components is one of the reasons for the recent popularity of holographic interferometry.

To the author's knowledge, neither holographic nor classical interferometers are available commercially as pre-designed units. They must be assembled from individual components purchased from optical equipment suppliers. Suitable optical elements, lens mounts, low vibration optical benches and lasers can be purchased from a wide range of sources, such as Mels Griot (www.mellesgriot.com), Edmund Industrial Optics (www.edmundoptics.com) and Esco Products (www.escoproducts.com).

4. Recent developments

In this section, some recent advances in laser interferometry are reviewed. Research done by the author on the measurement of low heat transfer rates in a two-dimensional temperature field will be described. Also, some of the recent literature on the application of interferometry to three-dimensional temperature fields will be covered. It should be mentioned that this is not a comprehensive review of recent developments. There are other active areas of research which will not be discussed, such as the application of interferometry in the presence of strong refraction effects (e.g., Lacona and Taine, 2001; Dietz and Balkowski, 1997).

4.1. Measurement of low convective heat transfer rates

The standard analysis method for the measurement of heat transfer utilizes temperature profile extrapolation. In this procedure the fluid temperature is calculated at specific locations, usually at points of maximum constructive and destructive interference i.e., at the fringe centers. Using these discrete temperature profile data, a curve-fitting algorithm is used to calculate the temperature gradient normal to the surface, from which the local convective heat transfer rate is calculated.

Small phase differences can be measured using specialized optical methods (Slepicka and Cha, 1995; Breuckmann and Thieme, 1985). But when interference patterns are recorded on film, several fringes are needed near the surface in order to characterize the near wall temperature profile. Unfortunately, because of the large variation in local heat transfer rates that is often encountered in a single experimental model, this is not always possible. Often, in regions with low local heat transfer rates there is insufficient fringe shift close to the surface, making it difficult to get the necessary data for accurate gradient estimation. To overcome this difficulty, Naylor and Duarte (1999) have developed a technique to measure the gradient directly from the interference fringe field.

To measure the surface temperature gradient directly, the interferometer is operated in the wedge fringe mode. Consider a measurement being made on an isothermal vertical surface with temperature T_s, as shown in Fig. 3. In this mode, a constant wedge fringe field is superimposed upon the fringe field produced by the near-wall temperature variation. For this setting, when the undisturbed wedge fringes in the ambient (T_∞) are perpendicular to the vertical surface, it is assumed that the interferometer is set such that a negative temperature gradient in the x-direction will cause the fringes to bend downward as they approach the surface. It should be noted that whether the wedge fringes bend upward or downward can be set by the experimenter, depending on the angle of the test beam relative to the reference beam (for a classical interferometer).

Naylor and Duarte (1999) have shown that the local temperature gradient on an isothermal surface can be obtained by measuring the angle (α) between the a line of constant fringe order and the surface. For an ideal gas, they have shown that the local convective heat transfer coefficient (h) is given by:

$$h = \frac{q}{(T_s - T_\infty)} = \frac{k_S R \lambda_o T_s^2}{LPG(T_s - T_\infty)\,\mathrm{d}\tan\alpha} = \frac{C}{\tan\alpha} \qquad (1)$$

where q is the convective heat transfer rate from the surface, k_S is the gas thermal conductivity, P is the absolute gas pressure, R is the gas constant, L is the length of the model in the beam direction, λ_o is the light vacuum wavelength, G is the Gladstone-Dale constant and d is the wedge fringe spacing. Note that $C = (k_S R \lambda_o T_s^2)/(LPG(T_s - T_\infty)d)$ is a constant for a given interferogram. Fig. 4 shows the variation of the heat transfer coefficient (h) with fringe angle (α). Eq. (1) and Fig. 4 apply only for an isothermal boundary. For a

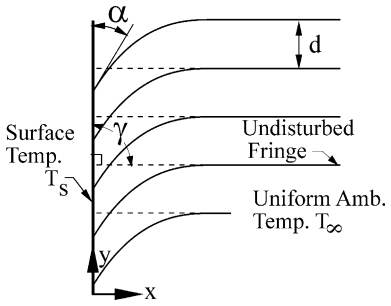

Fig. 3. Sketch of a wedge (finite) fringe pattern near a surface (Naylor and Duarte, 1999).

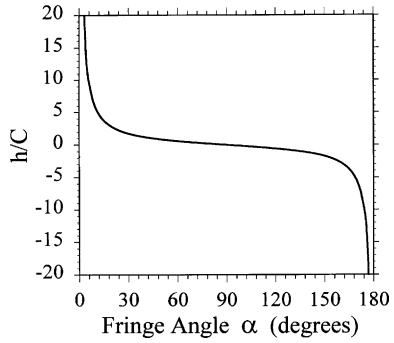

Fig. 4. Variation of the local convective heat transfer coefficient with fringe angle (Naylor and Duarte, 1999).

non-isothermal surface, the surface temperature gradient in the y-direction affects fringe intersection angle (α) and the analysis must be slightly modified (see Naylor and Duarte, 1999).

Fig. 5 shows a sample application for this "direct gradient method". Fig. 5(a) shows an infinite fringe interferogram and Fig. 5(b) shows the same experimental conditions taken in wedge fringe mode. These are interferograms of the temperature field in air adjacent to an indoor window glazing with a venetian blind. The blind slats are heated electrically to simulate solar heating. Note that in the middle and upper part of the interferogram, there is insufficient fringe shift near the window surface to obtain reliable measurements using traditional methods. However, in the wedge fringe interferogram the variation of the fringe angle (α) at the window surface is clearly visible. Naylor and Duarte (1999) have shown that measurement of the fringe angle is an effective method of obtaining local heat transfer rates in regions of low gradient. In addition, this approach also allows visualization of the local heat transfer distribution on a surface. Referring to Fig. 5(b), on the lower part of the window the fringe angle (α) is less than 90°, indicating that heat is being transferred from the window to the air. Further up the window the fringes intersect the surface at almost 90°, showing that the surface is nearly adiabatic in this region. At the top of the interferogram, the heated blind slats are hotter than the window surface. This causes the fringe intersection angle to be greater than 90°, revealing that direction of convective heat flow has reversed. Note that since the surface to ambient temperature difference remains positive, the heat transfer coefficient (as defined in Eq. (1)) is positive over the lower part of the window and negative over the upper section of the window.

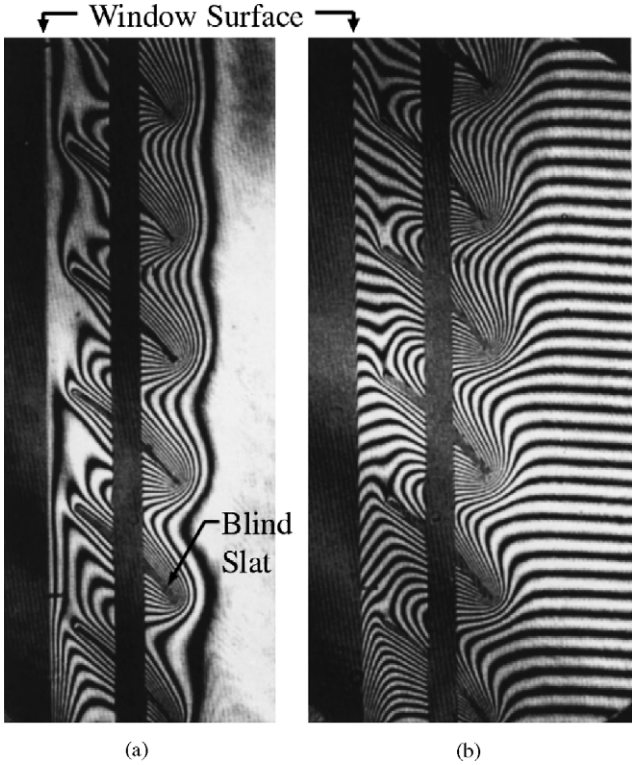

Fig. 5. (a) Infinite and (b) wedge fringe interferograms of free convection from an window glazing with a heated venetian blind, illustrating an application for the direct gradient method (Duarte et al., 2001).

4.2. Measurements in three-dimensional fields using interferometric tomography

Consider the asymmetric phase object with a refractive index field $n(x,y)$, shown in Fig. 6. In tomographic interferometry, the three-dimensional field is obtained usually by reconstructing the two-dimensional field in several $z=$ constant planes. The fringe order (ε) depends on the integral of the refractive index field $n(x,y)$ as follows:

$$\varepsilon(p,\theta)=\frac{1}{\lambda_o}\int\int((n(x,y)-n_{ref})\delta[p-r\sin(\phi-\theta)])\,dx\,dy \quad (2)$$

For a given observation angle (θ), $\varepsilon(p,\theta)$ is the fringe order that can be read from the interferogram. Note that

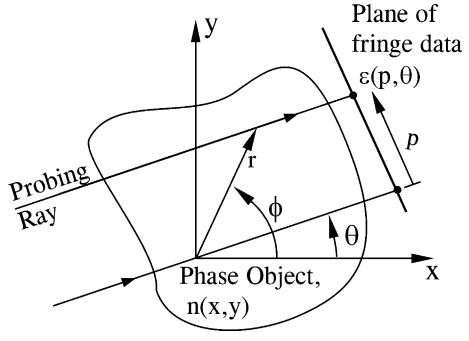

Fig. 6. Notation and coordinate system for interferometric tomography. Adapted from Vest (1979).

δ is the Dirac delta function. So, the integral in Eq. (2) represents the line integral of the refractive index variation along a probing light ray. It is important to note that Eq. (2) neglects the effects of ray curvature caused by refraction. When the length of the test section is long in the beam direction or the refractive index gradients are large normal to the beam, refraction may not be negligible. A discussion of refraction errors (and corrections) is given by Vest (1979) and Hauf and Grigull (1970).

For a general three-dimensional field, inversion of this line integral transform is not possible from a single interferogram. Estimation of the refractive index field requires several interferograms, each recorded at a different viewing angle relative to the phase object. Tomographic methods are then applied to the two-dimensional projections from the multiple views to reconstruct the refractive index field. The more general problem of reconstructing fields from their line integrals arises in a number of different fields (e.g. X-ray imaging and radio astronomy) and there is a great deal of literature on inversion techniques. A discussion of the fundamentals of interferometric tomography (IT) can be found in the text by Vest (1979).

Cha and Cha (1996) have noted that current reconstruction methods can be classified in two groups: (i) transform methods and (ii) series expansion methods. Transform methods require complete unblocked projections and a full angle of view of 180°, and have not been widely used in convective heat transfer. In contrast, series expansion methods can, in principle, deal with the limited data sets that are often encountered in practical heat transfer applications.

As previously mentioned, in tomographic interferometry the three-dimensional field is usually assembled by "stacking up" several reconstructed two-dimensional planes. For the series expansion method, each plane of the phase object is discretized into rectangular elements (or bases) and the refractive index field is approximated by a series, as follows:

$$n(x,y) - n_{\text{ref}} = \sum_{i=1}^{N} c_i f_i(x,y) \tag{3}$$

where $f_i(x,y)$ are the series expansion basis functions, c_i are the unknown coefficients and N is the number of elements. The series expansion method described by Vest (1979) uses a uniform element size with a constant value assigned to the refractive index within each element. As shown in Fig. 6, the fringe data is measured as a function of the projection angle (θ) and the distance from the optical axis (p). The coefficients (c_i) are determined by solving the system of linear algebraic equations given by:

$$\varepsilon(p_j,\theta_j) = \frac{1}{\lambda_o} \sum_{i=1}^{N} c_i \phi_i(p_j,\theta_j) \tag{4}$$

where $\phi_i\ (p_j,\theta_j)$ is the line integral transform of $f_i(x,y)$ and the subscript j represents the number of measurement points i.e., number of probing light rays. In other words, Eq. (4) is a series approximation to Eq. (2), which is the integral along a probing ray. Often, the number of measurement points exceeds the number of unknown coefficients and the simultaneous equations are solved in a least-squares sense.

There have been several successful applications of interferometric tomography (IT) to convective heat transfer problems. One of the earliest applications of IT to convective heat transfer was done by Sweeney and Vest (1974). In this study, IT was used to study the thermal plume above a horizontal heated rectangular plate. Diffuse illumination holographic interferometry was used to obtain data at an effective viewing angle of 60°. In this work, the temperature field was reconstructed in several horizontal planes, but no heat transfer data were obtained.

In a more recent study, Bahl and Liburdy (1991) used IT to reconstruct the instantaneous unsteady temperature field above a horizontal heated circular disk. The diameter of the heated section of the disc was 50.8 mm. Fig. 7 shows the optical setup of the holographic interferometer. This figure shows that diffuse illumination holography was used to obtain fringe data simultaneously with a viewing angle of 60°, plus an additional view at 90° to the central viewing direction. For some measurements, data from a total of 15 viewing directions over the 60° viewing angle (plus the 90° view) were used to reconstruct the temperature field. An iterative series expansion method was used to reconstruct the temperature distributions in three horizontal planes.

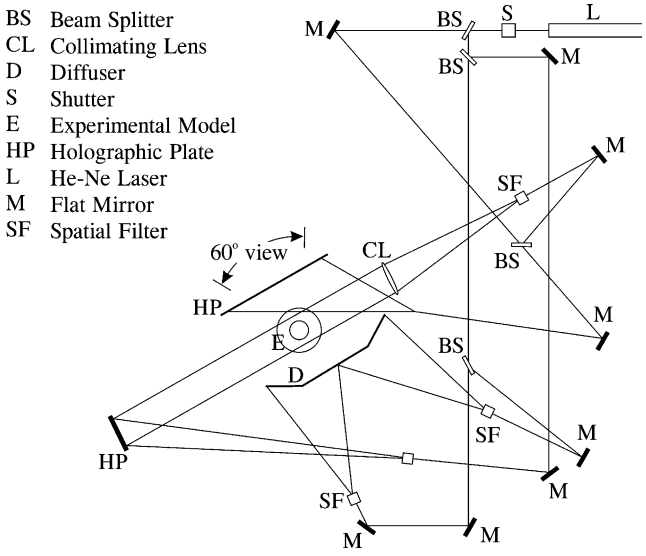

Fig. 7. Optical setup used by Bahl and Liburdy (1991) for diffuse illumination holographic interferometry.

Fig. 8 shows the local heat transfer coefficient distribution on the disk obtained by extrapolation.

Mishra et al. (1999) have used tomography to study Rayleigh–Benard convection in a horizontal bottom-heated enclosure with air as the test fluid. The enclosure was 500 mm × 500 mm in plan with the cavity depth being adjustable. Interferograms were obtained with a 70 mm beam diameter MZI in the infinite fringe mode. Data were collected at six viewing angles over a total view of 150°. Fig. 9 shows the local Nusselt number distributions over the upper and lower cavity surfaces at a Rayleigh number (based on the gap width) of $Ra = 13{,}900$. At this Rayleigh number, the upper wall was cooled to a temperature of 13.4 °C and the lower wall was heated to 30.5 °C, with a cavity depth of 20 mm.

The studies discussed above considered problems for which the view of the phase object was completely or largely unobstructed. But for many geometries, the opaque test model will partially block the view in most of the viewing directions. In such cases, the reconstruction problem is substantially more difficult. Cha and Cha (1996) have tackled this challenging problem, reconstructing the steady three-dimensional free convective temperature field about two interacting isothermal cubes. The heated cubes (side length of about 2.5 cm) were immersed in a tank of glycerin with dimensions $25.4 \times 25.4 \times 35.6$ cm. The relative positions of the thermally interacting cubes are shown in Fig. 10. Fig. 11 shows an infinite fringe interferogram of the two cubes. In this study, the temperature field was reconstructed in horizontal plane A–A, as marked in Figs. 10 and 11. To handle this problem, Cha and Cha (1995b) have developed a series expansion method that makes use of a variable grid. The variable grid method uses finer

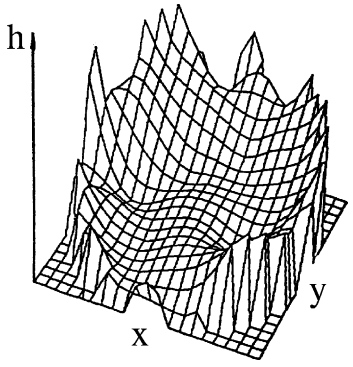

Fig. 8. Measured local heat transfer coefficient distribution on a 50.8 mm diameter horizontal disk, obtained using interferometric interferometry (Bahl and Liburdy, 1991). Reproduced with permission of Elsevier Ltd.

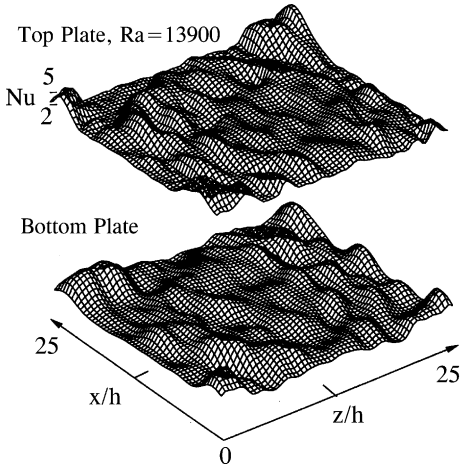

Fig. 9. Local Nusselt number distribution in a horizontal enclosure with Rayleigh–Benard convection, $Ra = 13{,}900$ (Mishra et al., 1999). Reproduced with permission of Elsevier Ltd.

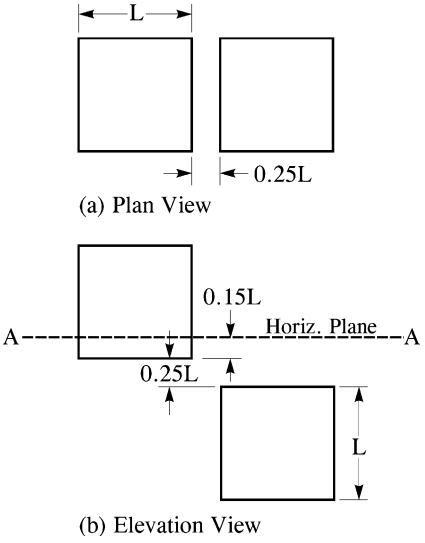

Fig. 10. Plan and elevation views showing the configuration of the two cubes studied by Cha and Cha (1996).

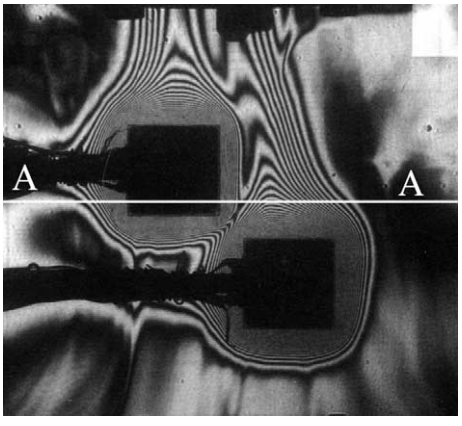

Fig. 11. Infinite fringe interferogram of free convection from two isothermal cubes in glycerin, $Ra \cong 1300$ (Cha and Cha, 1995a). Reproduced with permission of Elsevier Ltd.

elements in regions that are heavily scanned by probing rays, resulting in enhanced reconstruction accuracy and resolution, compared to a uniform grid method. Data was obtained at 10° increments over the full 180° view by rotating the test section and taking interferograms using double exposure holographic interferometry. Fig. 12 shows the reconstruction of plane A–A using data from the complete range of viewing angles (180°), compared to the form of the actual temperature field, obtained numerically. It can be seen that the general form of the refractive index field has been recovered. However, near the isothermal surface, there are substantial errors because this region is probed by a very limited number of rays. In addition, when the total viewing angle was reduced from 180° to 40°; Cha and Cha (1996) found that the reconstructed field became much less accurate, even well away from the opaque cube surfaces.

In the study by Cha and Cha (1996) heat transfer data were not presented. However, the same tomographic method was recently used to measure the con-

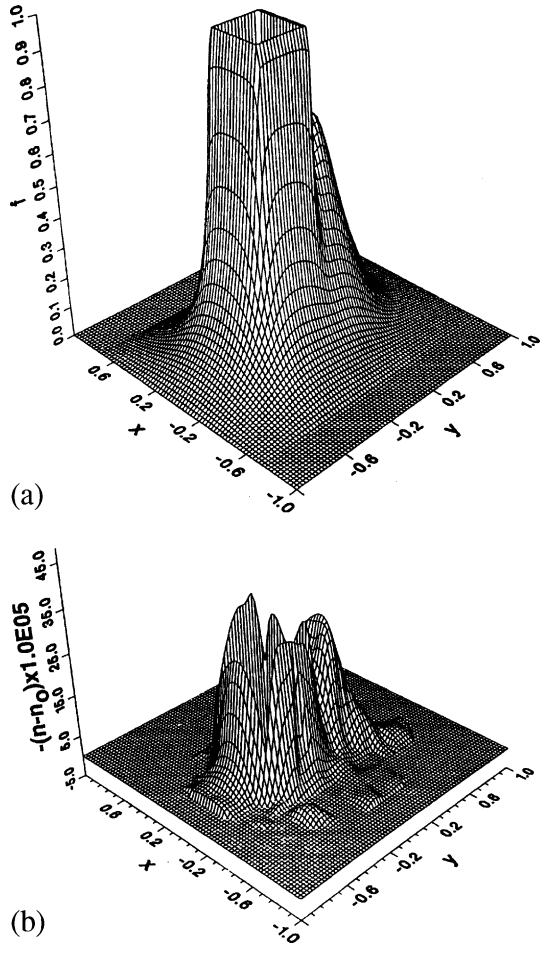

Fig. 12. (a) Numerically computed temperature field in plane A–A, and (b) the tomographic reconstruction of the refractive index field in plane A–A using a full 180° view (Cha and Cha, 1996). Reproduced with permission of AIAA.

vection from an isolated cube by Cha and Hwang (1999). In this work, face-averaged Nusselt numbers were reported, which compared well with numerical simulations and empirical correlations.

It is clear from the above discussion that IT has some limitations, especially when applied to opaque test objects that significantly obstruct the near-wall view. Although average heat transfer data measurements have been made using IT, local heat transfer coefficients are reported less frequently. Also, it should be noted that a viscous test fluid (glycerin) was used in the study by Cha and Cha (1995a, 1996). This yielded a low Rayleigh number and thick thermal boundary layers. One would expect that reconstruction of the temperature field in water under similar thermal conditions would be more difficult because of the thinner boundary layers.

4.3. Beam-averaged local heat transfer measurements

As previously noted, for a general three-dimensional field, the temperature distribution cannot be determined from a single interferogram. However, for some geometries, it is possible to determine the mean temperature and heat transfer rate, averaged in the direction of the light beam. Beam-averaged measurements have been reported in several recent publications (Kato and Maruyama, 1989; Li and Tarasuk, 1992; Fehle et al., 1995; Lai and Naylor, 2002). Although such measurements are intrinsically approximate when the measurement surface is not isothermal, this approach requires much less computational effort than tomography. Also, beam-averaged measurements can often be made in situations where the viewing angle is highly restricted and tomography is not possible.

Two applications of this method are shown in Fig. 13. Fig. 13(a) shows an infinite fringe interferogram of free convection over an upward-facing heated flat plate that is inclined at 18.5° with respect to horizontal ($Gr = 1.25 \times 10^8$). Fig. 13(b) shows an interferogram of developing free convection in a square heated duct, inclined at 45° with respect to gravity. To obtain these images, the light beam was directed parallel to the primary flow. In this configuration, the interferometer integrates changes in refractive index from the inlet to the outlet of the experimental model, such that each fringe represents approximately a line of constant axially averaged temperature. Note that the effect of secondary flow on the temperature field can be seen in both Fig. 13(a) and (b). It should also be mentioned that, although the sections of Fig. 13(b) with high fringe density appear blurred and gray in the reproduced image, distinct fringes are clearly visible in the original image under appropriate magnification. This interferogram was recorded on large format (10×13 cm) high resolution film (400 lines/mm) which allows for accurate quantitative analysis.

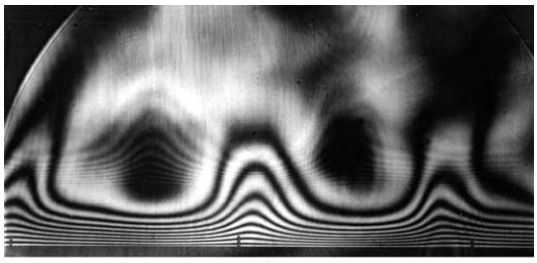

(a)

(b)

Fig. 13. Beam-averaged interferograms of (a) free convection from a heated upward-facing isothermal plate inclined at 18.5° to horizontal (Lai and Naylor, 2002), and (b) developing free convection in a square duct inclined at 45° to the horizontal (Papple and Tarasuk, 1987). Reproduced with permission of AIAA.

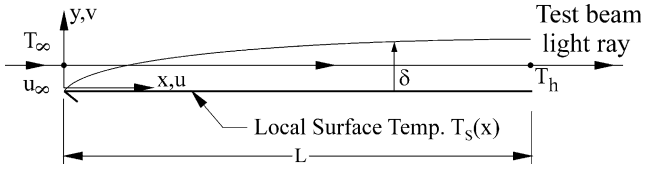

Fig. 14. Thermally developing flow over a surface with a temperature variation in the light beam direction (Naylor and Machin, 2001).

To analyze this problem, consider a thermally developing flow of an ideal gas over a non-isothermal surface of length L, as shown in Fig. 14. The surface temperature T_s varies in the direction of the light beam i.e., the x-direction. The light beam enters the test section at temperature T_∞ and exits at temperature T_h. Because of the non-linear variation of refractive index with temperature, when there is a temperature variation in the direction of the light beam, the temperature that should be assigned to an interference fringe is not the average gas temperature. The effective fringe temperature can be derived as follows (Naylor and Machin, 2001):

Consider a ray of light in the object beam passing at a distance y above the surface shown in Fig. 14. Neglecting refraction effects, for an ideal gas the fringe shift order $\varepsilon(y)$ is related to the refractive index field $n(x,y)$ as follows:

$$\varepsilon(y) = \frac{1}{\lambda_o}\int_0^L (n(x,y) - n_{ref})\,dx = \frac{PGL}{R\lambda_o}\int_0^1 \left(\frac{1}{T(x^*,y)} - \frac{1}{T_{ref}}\right)dx^* \quad (5)$$

where T_{ref} is the reference temperature, L is the length of the test model in the light beam direction, P is the absolute gas pressure, R is the gas constant, G is the Gladstone-Dale constant and λ_o is the vacuum light wavelength. A dimensionless axial coordinate, $x^* = x/L$, has been introduced in Eq. (5).

Now consider the hypothetical uniform temperature along the light ray, T_f, that would produce same the fringe shift $\varepsilon(y)$ as the non-uniform distribution, $T(x^*,y)$. With this uniform temperature, the fringe shift is:

$$\varepsilon(y) = \frac{PGL}{R\lambda_o}\int_0^1 \left(\frac{1}{T_f} - \frac{1}{T_{ref}}\right)dx^* = \frac{PGL}{R\lambda_o}\left(\frac{1}{T_f} - \frac{1}{T_{ref}}\right) \quad (6)$$

Equating Eqs. (5) and (6) and simplifying gives:

$$T_f = \left[\int_0^1 \frac{1}{T(x^*,y)}dx^*\right]^{-1} \quad (7)$$

In Eq. (7), T_f is the effective temperature that should be assigned to a fringe when the temperature varies in the object beam direction (x^*). But, in general, $T(x^*,y)$ is not known and cannot be determined from a single interferogram. The approach taken to overcome this difficulty in many previous studies has been to assume that T_f is equal to the arithmetic average fluid temperature. With this approximation, it follows from Eq. (6) that:

$$\overline{T} \cong T_f = \frac{T_{ref}}{1 + \varepsilon R\lambda_o T_{ref}/PGL} \quad (8)$$

Eq. (8) can be used to evaluate the effective fringe temperature for known experimental conditions. However, it is evident from Eq. (7) that the effective fringe temperature T_f is not precisely the arithmetic average of $T(x^*,y)$. Recently, Naylor and Machin (2001) have analyzed this source of error for a range of conditions that are commonly used in convective heat transfer experiments. The measured average temperature (T_f) was compared to the actual average fluid temperature ($\overline{T}$). The study considered a power function and periodic temperature variations in the beam direction, with water and ideal gases as the test fluids. Fig. 15 shows some of the results of this analysis for measurements made in ideal gases. In Fig. 15, the temperature variation along the light beam is assumed to be proportional to x^m. It can be seen that the difference between the measured average fluid temperature (T_f) and the actual average fluid temperature ($\overline{T}$) is less than 2% of the overall temperature difference along the beam ($T_h - T_\infty$), even for the most adverse form of temperature distribution in the light beam direction. In fact, for many commonly

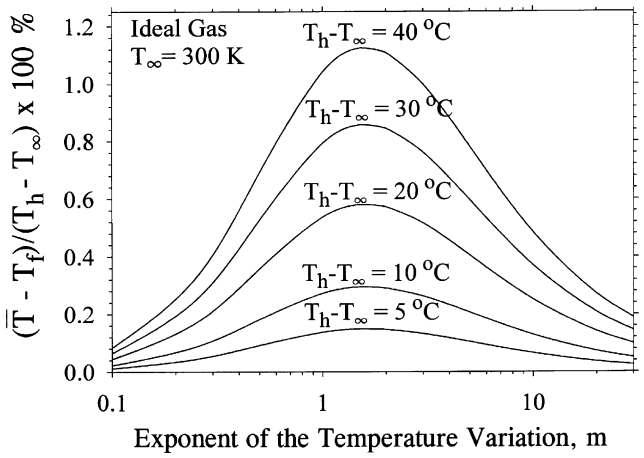

Fig. 15. Percentage difference between the measured fringe temperature and the true beam-average temperature (Naylor and Machin, 2001).

encountered experimental conditions, the intrinsic error in the beam-averaged temperature field (calculated using Eq. (8)) was found to be less than 1%.

From the above result, one might be tempted to assume that the error in the beam-average heat transfer rate, calculated from the approximate temperature field measurements, will also be small. Unfortunately, it has been shown that this will not always be true. Recently, Naylor (2001, 2002) has performed an error analysis to determine the accuracy of beam-average heat transfer measurements made in ideal gases. Fig. 16 shows sample results from this study, which considered forced convection on a plate with a power function surface temperature variation of the form: $T_s = (T_L - T_\infty)x^n + T_\infty$., where T_∞ is the ambient temperature and T_L is the plate surface temperature at $x = L$. Fig. 16 shows the variation of the intrinsic error in the beam-averaged surface temperature gradient for a range of surface temperature differences. In Fig. 16, $d\overline{T}/dy|_{y=0}$ is the actual surface temperature gradient and $dT_f/dy|_{y=0}$ is the approximate surface gradient, calculated from the temperature field

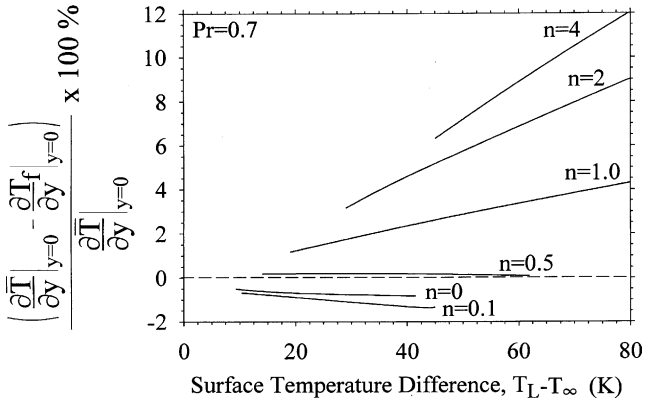

Fig. 16. Percentage error in the measured beam-averaged surface gradient for forced convection on a non-isothermal plate (Naylor, 2001).

measurements. The results show that the inherent error in the measurements depends strongly upon the form (n) and magnitude of the temperature variation in the light beam direction. Although the error in the measured heat transfer rate will be small for many commonly encountered conditions, Fig. 16 shows that it can be greater than 10% in extreme cases. So, caution must be used (and corrections considered) when applying this method on non-isothermal surfaces.

5. Concluding remarks

Laser interferometry continues to be an important experimental technique for convective heat transfer measurements. In this paper some of the recent developments in this field were presented. A technique for measuring low temperature gradients was discussed for two-dimensional fields. For three-dimensional fields, some recent publications in the field of interferometric tomography were reviewed. Although a very powerful technique, the literature shows that tomography has significant limitations for some convective heat transfer applications. Published results show that the accuracy of the reconstructed temperature field is reduced substantially when an opaque test model obstructs the view or when the viewing angle is limited. To conclude, an approximate beam-averaging approach for obtaining heat transfer rates in three-dimensional fields was discussed. This method does not require the high computational effort associated with tomography and can be applied for some geometries that are not amenable to tomographic analysis.

Acknowledgements

The author acknowledges the support of the Natural Sciences and Engineering Research Council of Canada.

References

Asseban, A., Lallemand, M., Saulnier, J.-B., Fomin, N., Lavinskaja, E., Merzkirch, W., Vitkin, D., 2000. Digital speckle photography and speckle tomography in heat transfer studies. Optics Laser Technol. 32, 583–592.

Bahl, S., Liburdy, J.A., 1991. Measurement of local convective heat transfer coefficients using three-dimensional interferometry. Int. J. Heat Mass Transfer 34, 949–960.

Breuckmann, B., Thieme, W., 1985. Computer-aided analysis of holographic interferograms using the phase-shift method. Appl. Optics 24, 2145–2149.

Cha, D.J., Cha, S.S., 1995a. Three-dimensional natural convection flow around two interacting isothermal cubes. Int. J. Heat Mass Transfer 38 (13), 2343–2352.

Cha, D.J., Cha, S.S., 1995b. Natural pixel decomposition for computation of tomographic reconstruction from interferometric projec-

tion: algorithms and comparison. SPIE Conference on Optical Techniques in Fluid, Thermal and Combustion Flow, vol. 2546, pp. 225–233.

Cha, D.J., Cha, S.S., 1996. Holographic interferometric tomography for limited data reconstruction. AIAA J. 34 (5), 1019–1026.

Cha, D.J., Hwang, H.S., 1999. Measurement of convective heat transfer from an isothermal cube using holographic interferometric tomography. SPIE Conference on Optical Diagnostics for Fluids/Heat/Combustion and Photomechanics for Solids, vol. 3783, pp. 165–174.

Dietz, G., Balkowski, I., 1997. Interferometry and reconstruction of strongly refracting fields in two-dimensional boundary layer flow. Exp. Fluids 12, 423–431.

Duarte, N., Naylor, D., Oosthuizen, P.H., Harrison, S.J., 2001. An interferometric study of free convection at a window glazing with a heated venetian blind. Int. J. HVAC&R Res. 7, 169–184.

Eckert, E.R.G., Soehngen, E.E., 1948. Studies on heat transfer in laminar free convection with the Mach–Zehnder interferometer. AF Technical Report 5747, United States Air Force, Wright Patterson AFB, Dayton, Ohio, pp. 1–21.

El Ammouri, F., Taine, J., 1994. Measurement of wall conductive heat flux in turbulent gas flow by laser beam deflection. Int. J. Heat Mass Transfer 37 (12), 1759–1771.

Fehle, R., Klas, J., Mayinger, F., 1995. Investigation of local heat transfer in compact heat exchangers by holographic interferometry. Exp. Therm. Fluid Sci. 10, 181–191.

Fröhlich, T., Guenoun, P., Bonetti, M., Perrot, F., Beysens, D., Garrabos, Y., Le Neindre, B., Bravais, P., 1996. Adiabatic versus conductive heat transfer in off-critical SF6 in the absence of convection. Phys. Rev. E 54 (2), 1544–1549.

Goldstein, R.J., 1970. Optical measurement of temperature. In: Measurement Techniques in Heat Transfer, Technivision Services, Slough, England, pp. 177–228.

Guo, Z.-Y., Song, Y.-Z., Li, Z.-X., 1995. Laser speckle photography in heat transfer studies. Exp. Therm. Fluid Sci. 10, 1–16.

Hauf, W., Grigull, U., 1970. Optical methods in heat transfer. In: Harnett, J.P.Irvine Jr., T.F. (Eds.), Adv. Heat Transfer, vol. 6. Academic Press, New York, pp. 133–366.

Herman, C., Kang, E., 2001. Comparative evaluation of three heat transfer enhancement strategies in a grooved channel. Heat Mass Transfer 37, 563–575.

Iida, T., Murakami, M., Shimazaki, T., Nagai, H., 1996. Visualization study on the thermo-hydrodynamic phenomena induced by pulsative heating in He II by the use of a laser holographic interferometer. Cryogenics 36 (11), 943–949.

Inada, S., Taguchi, T., Yang, W.-J., 1999. Effects of vertical fins on local heat transfer performance in a horizontal fluid layer. Int. J. Heat Mass Transfer 42, 2897–2903.

Kato, S., Maruyama, N., 1989. Holographic interferometric measurements of the three-dimensional temperature field with thermally developing flow in the measuring-beam direction. Exp. Therm. Fluid Sci. 2, 333–340.

Kennard, R.B., 1939. Temperature distribution and heat flux in air by interferometry. Temperature: Its Measurement and Control in Science and Industry. Reinhold Publishing Corp., New York, pp. 685–706.

Kreis, T., 1996. Holographic Interferometry—Principles and Methods. Akademie Verlag, Berlin.

Kwak, C.E., Song, T.H., 2000. Natural convection around horizontal downward-facing plate with rectangular grooves: experiments and numerical simulations. Int. J. Heat Mass Transfer 43, 825–838.

Lacona, E., Taine, J., 2001. Holographic interferometry applied to coupled free convection and radiative heat transfer in a cavity containing a vertical plate between 290 and 650 K. Int. J. Heat Mass Transfer 44, 3755–3764.

Lai, B.Y., Naylor, D., 2002. Measurement of the spanwise free convective heat transfer distribution on an inclined upward-facing heated plate. 12th International Heat Transfer Conference, Grenoble, France, vol. 2, pp. 645–650.

Li, J., Tarasuk, J.D., 1992. Local free convection around inclined cylinders in air: an interferometric study. Exp. Therm. Fluid Sci. 5, 235–242.

Liou, Y.-M., 2001. Some applications of experimental and numerical visualization in fluid flow, heat transfer and combustion. Exp. Therm. Fluid Sci. 25, 359–375.

Mayinger, F., 1994. Fundamentals of holography and interferometry. In: Mayinger F. (Ed.), Optical Methods–Techniques and Applications, Springer-Verlag, New York, pp. 27–50 (Chapter 4).

Mishra, D., Muralidhar, K., Munshi, P., 1999. Experimental study of Rayleigh–Benard convection at intermediate Rayleigh numbers using interferometric tomography. Fluid Dynam. Res. 25, 231–255.

Nakano, A., Shiraishi, M., Murakami, M., 2001. Application of laser holography interferometer to heat transport phenomena near the critical point of nitrogen. Cryogenics 41, 429–435.

Naylor, D., 2001. An error analysis of beam-averaged interferometric heat transfer measurements. International Mechanical Engineering Congress and Exposition. ASME Paper HTD-24409, pp. 1–8.

Naylor, D., 2002. On the accuracy of beam-averaged interferometric heat transfer measurements. J. Heat Transfer 24 (5), 1072–1077.

Naylor, D., Duarte, N., 1999. Direct temperature gradient measurement using interferometry. Exp. Heat Transfer 12, 279–294.

Naylor, D., Machin, A.D., 2001. The accuracy of beam-averaged interferometric temperature measurements in a three-dimensional field. Exp. Heat Transfer 14 (3), 217–228.

Papple, M.C.L., Tarasuk, J.D., 1985. Natural convection about vertical cylinders immersed in a variable property gas. ASME/AICHE National Heat Transfer Conference, paper 85-HT-15, pp. 1–8.

Papple, M.C.L., Tarasuk, J.D., 1987. An interferometric study of developing natural convective flow in inclined isothermal ducts. AIAA 22nd Thermophysics Conference, Hawaii, Paper 87-1589, pp. 1-8.

Ramesh, N., Merzkirch, W., 2001. Combined convective and radiative heat transfer in side-vented open cavities. Int. J. Heat Fluid Flow 22, 180–187.

Shakher, C., Nirala, A.K., 1999. A review on refractive index and temperature profile measurements using laser-based interferometric techniques. Optics Lasers Eng. 31, 455–491.

Sheng-jie, X., 1983. Double mirror laser interferometer. Proceedings of the Third International Conference on Flow Visualization, Ann Arbor, Michigan, USA, pp. 155–159.

Slepicka, J.S., Cha, S.S., 1995. Stabilized nonlinear regression for interferogram analysis. Appl. Optics 34, 5039–5044.

Sweeney, D.W., Vest, C.M., 1974. Measurements of three-dimensional temperature fields above heated surfaces by holographic interferometry. Int J. Heat Mass Transfer 17, 1443–1454.

Tanda, G., 1993. Natural convection heat transfer from a staggered vertical plate array. J. Heat Transfer 115, 938–945.

Vest, C.M., 1979. Holographic Interferometry. John Wiley & Sons, New York.

Wozniak, K., Siekmann, J., 1995. Benard-convection analysis using a new interferometer. Flow Meas. Instrum. 6 (3), 181–186.

Yan, D., Cha, S.S., 1998. Practical common-path interferometry for real-time thermal/fluid flow measurements. Int. Commun. Heat Mass Transfer 25 (1), 1–8.

Yoon, J.I., Moon, C.G., Kim, E., Son, Y.S., Kim, J.D., Kato, T., 2001. Experimental study on freezing of water with supercooled region in a horizontal cylinder. Appl. Therm. Eng. 21, 657–668.

Zhang, L., Petit, J.-P., Taine, J., 1989. Measurements of temperature profiles in gases by laser beam deflection. Rev. Phys. Appl. 24, 401–410.